THE STRUCTURE OF THE MIDDLE CORONA FROM OBSERVATIONS AT 80 AND 160 MHz

G. A. DULK* and K. V. SHERIDAN
Division of Radiophysics, CSIRO, Sydney, Australia

(Received 31 December, 1973)

Abstract. Maps of the brightness distribution of the 'quiet Sun' at 80 and 160 MHz reveal the presence of features both brighter and darker than average. The 'dark' regions are well correlated with dark regions on UV maps; we deduce that they result from 'coronal holes'. The 'bright' regions are associated with quiescent filaments and not plages or bright regions on microwave or UV maps; we deduce that they result from 'coronal helmets'.

When coronal holes appear near the centre of the disk we can estimate the density and kinetic temperature in the holes from the radio observations. For a hole observed on 1972 July 20–21, we find $T \approx 0.8 \times 10^6$ inside the hole and $T \approx 1.0 \times 10^6$ in average regions outside the hole. Inside the hole the density is estimated to be about one-quarter of that in Newkirk's model of the spherically symmetric corona.

Variations in brightness at a fixed height above the limb are generally well correlated with scans at a similar height made with a K-coronameter. Occasional differences may result from streamers protruding beyond the limb from the back of the Sun. These can be seen by the K-coronameter but, because of refraction of the radio rays, not by the radio-heliograph.

1. Introduction

The structure of the Sun's corona has recently been observed in many parts of the electromagnetic spectrum: X-rays (Vaiana *et al.*, 1973a, 1973b), UV (Withbroe *et al.*, 1971; Withbroe, 1972), visible (Hansen *et al.*, 1972; Altschuler *et al.*, 1972), short radio waves (Hobbs *et al.*, 1973; Kundu, 1971) and long radio waves (Leblanc, 1970; Aubier *et al.*, 1971; Sheridan, 1970). As a result of these studies it has now become possible to study coronal structures such as helmets, streamers, condensations and holes on the disk as well as at the limb. Some of these structures are localized in the low corona while others extend to great heights; some of the latter features can manifest themselves in metre-wavelength radio waves. We now present some observations of the corona at 160 and 80 MHz, and compare the structures with those seen at UV and visible wavelengths.

2. Observations

Radioheliograms of the quiet Sun are recorded with the Culgoora radioheliograph at 80 and 160 MHz (Sheridan *et al.*, 1973) several times a day whenever the Sun is free from strong non-thermal sources. Best results are obtained when the Sun is near the meridian and ionospheric refraction is a minimum. At 160 MHz the beamwidth is 1'.9 by 1'.9 sec (Z), where Z is the zenith angle of the Sun. At 80 MHz the beamwidth is

* Exchange visitor from the Dept. of Astro-Geophysics, Univ. of Colorado, Boulder, U.S.A.

Solar Physics **36** (1974) 191–202.

twice as large. Series of about 60 one-second radioheliograms at both 80 and 160 MHz are recorded on magnetic tape and are later processed on a computer, as follows.

(1) The individual radioheliograms (both polarizations) are added together to increase the signal-to-noise ratio.

(2) The data are smoothed by removing all spatial frequency components above the cutoff of the array and applying a cosine 'bell' to the lower-frequency components. This procedure increases the effective beamwidth by about 20%. Further cleaning procedures to correct for sidelobes cannot be used (at least at 160 MHz) because the beam pattern is not known over the required area. (At 160 MHz the picture field covers about 1° while the quiet Sun extends almost to the edge of the picture. For proper correction of sidelobes, the beam pattern must be known over an area about four to nine times the area of the source.)

(3) Minor instrumental effects (such as offsets, gain variations, etc.) introduced by the heliograph are removed and a contour map is plotted.

The quality of the resulting contour maps depends mainly on the sidelobe level of the radioheliograph beams. This is because the Sun is of large angular extent, ~ 500 beam areas at 160 MHz. At a given position the observed brightness is the true brightness convolved with the beam pattern. Even if the sidelobe level is only a few per cent the convolution can lead to large errors when the angular size of the source is large. A low sidelobe level requires that the phase errors in the radioheliograph be small, a condition which is difficult to maintain. For these reasons we have had only a few periods of a week or more when a suitably low sidelobe level coincided with a sufficiently low level of transient solar activity to allow meaningful quiet Sun observations. One such period, from 1972 July 13 to 21 will now be discussed.

3. Results

3.1. Contour maps

Figures 1a and 1b show sequences of radioheliograms at both 80 and 160 MHz, together with magnetic field maps from Mount Wilson, and maps made in the 284 Å Fe XV line by the NASA experiment on OSO-7 (*Solar-Geophysical Data*, 1972). Inspection of these maps shows the following highlights.

(1) In agreement with earlier, one-dimensional radio observations (Avignon and Le Squeren-Malinge, 1961) the general shape of the brightness distributions tends to be elliptical or rectangular, elongated parallel to the equator. The outer contours have similar shapes at 80 MHz, 160 MHz and in the UV at 284 Å – e.g., in Figure 1a the equatorial bulges above the west limb cover a greater latitude range than in the East and there is a pronounced valley in the south-east. The brightness distributions tend to have a flat top (especially at 160 MHz) with one or several peaks superimposed. The brightness drops rapidly near the half-intensity point but then there is a fairly extended skirt.

(2) The peaks on the radio maps are about 10–30% brighter than the average level. Their positions are often similar at 80 and 160 MHz, and they can be followed day by

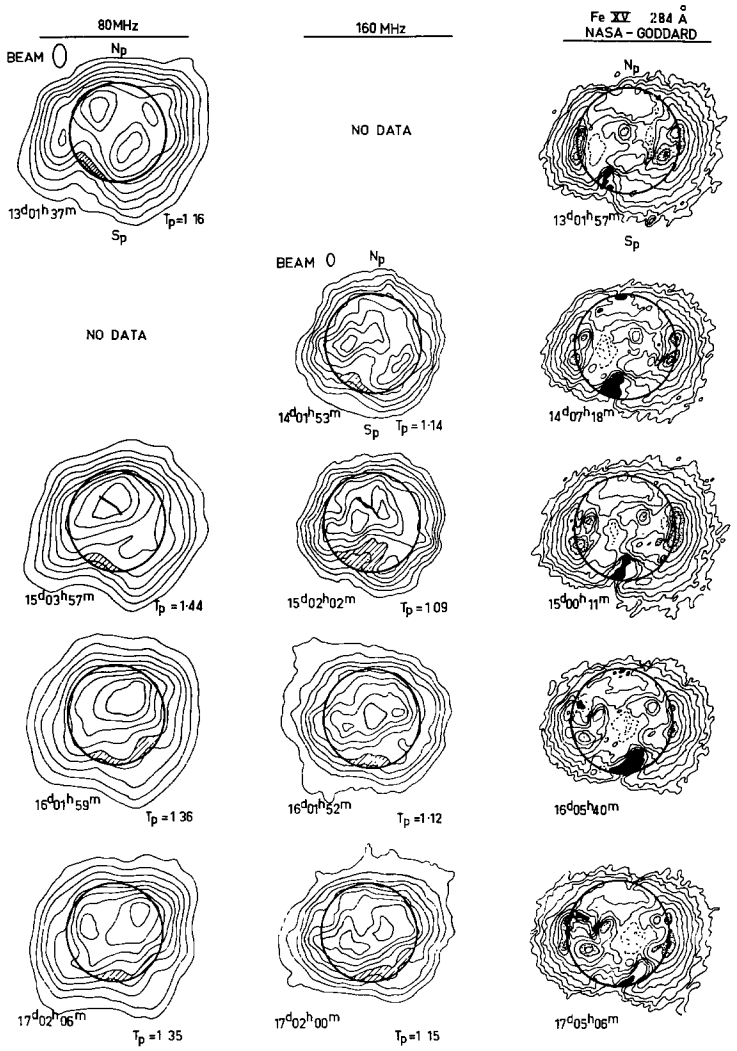

Fig. 1a.

Fig. 1a–b. Maps of coronal brightness observed, in 1972 July, by the Culgoora radioheliograph at 80 and 160 MHz and by the spectroheliograph on OSO-7 in the UV line of Fe xv at 284 Å. Figure 1b also includes the Mt. Wilson magnetograms. The circles represent the visible disk. The radio contours represent 0.1, 0.2,.... 0.9 of T_p (units of 10^6 K), the peak beam brightness temperature of the map. Dashed lines indicate depressions. On the radio maps, the hatching emphasizes regions on the disk which are unusually dark. On the UV maps, the stippled areas emphasize the brightest regions, above contour 640, and the blackened areas on the disk emphasize the darkest regions, below contour 10. The dark-line segments on the maps of July 15 show the position of a quiescent filament.

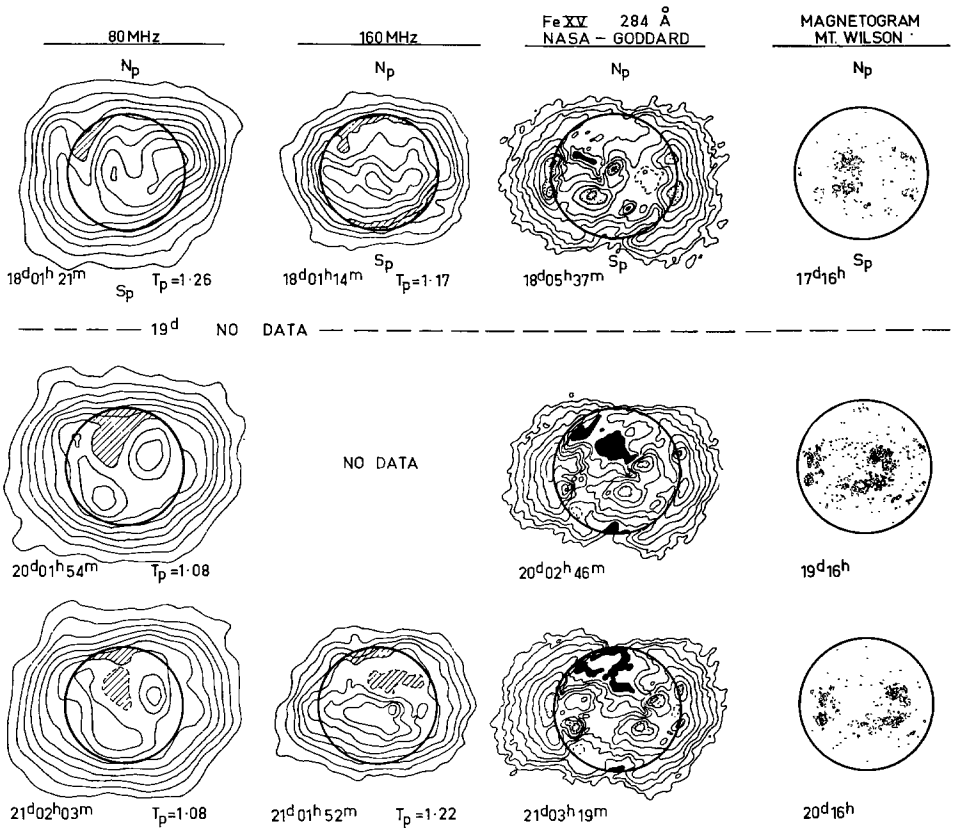

Fig. 1b.

day as the Sun rotates. We have compared the positions of the metre wavelength enhancements with plages, magnetic field enhancements and the bright regions seen in the UV maps on Figure 1, but we find little or no correspondence. Similarly, there is little correlation with the bright regions seen on the Fleurs 21-cm radio maps or the Stanford 9- cm maps (*Solar-Geophysical Data*, 1972). There is, instead, a correlation with the position of quiescent filaments seen in Hα. The pronounced bright region crossing the disk between July 13 and 18 (Figure 1a) lies above an extended filament (depicted on the map of July 15) which is far from any active regions.

It is likely that many of the metre-wave radio enhancements result from coronal helmets which lie above the quiescent filaments. We will present a fuller discussion later.

(3) Possibly the most interesting features are the regions of relatively low brightness on the 80 and 160 MHz radio maps and their close association with the areas of low Fe XV emission. In Figure 1 such areas are emphasized with hatching or shading. In the radio maps, there may be actual minima in the brightness distribution (as on July 21, Figure 1b) or indentations in the contours (most prominent from July 13 to 15, Figure 1a). The observed depth of these depressions is about 10–30%.

It has been established that the depressions in brightness of UV spectroheliograms result from 'coronal holes', regions where the coronal density (and probably, temperature) is lower than normal (Withbroe *et al.*, 1971; Perry and Altschuler, 1973) and the chromosphere is void of all solar activity. We discuss the implications of their appearance on the radio maps below.

3.2. Correlation with K-coronal brightness above the limb

To compare our radio results with white-light observations, we plot in Figure 2 the brightness as a function of position angle at fixed heights. Radii of 1.2 $R_\odot$ for 160 MHz and 1.45 $R_\odot$ for 80 MHz were chosen because they are the radii of the respective plasma levels in Newkirk's (1961) model of a coronal active region; as seen in Figure 1, they are approximately the half-intensity heights. Because of apparent displacements of the Sun caused by ionospheric refraction, we centred the position angle scans on the centroid of brightness. In Figure 2 the radio scans are compared with scans of the polarized brightness at 1.57 $R_\odot$ made by the HAO K-coronameter at Mauna Loa, Hawaii (Hansen *et al.*, 1969). We note that there is fairly general agreement between the radio and optical curves, but there are differences in detail. All three curves, 80 MHz, 160 MHz and K-coronameter, show low brightness near the poles, generally higher brightness in the mid-latitude and equatorial regions, and locally high brightness in streamers. The coronal hole in the south-east (the valley near $PA = 160°$) can be seen to move westward from July 13 to 17.

Occasional peaks in the K-corona brightness which are not present in the radio data can be explained as follows: The radio brightness is proportional to the integral of N_e^2 along the refracted and scattered ray path. Near the perimeter of the radio Sun, because of the strong refraction, the regions which contribute most to the brightness lie on the front of the Sun (Smerd, 1950). On the other hand, the K-coronal brightness is proportional to the integral of N_e along an undeviated path through the corona. Therefore, streamers anchored beyond the limb can be seen with the K-coronameter but usually not with the radioheliograph. In addition, because of the different density dependence, a diffuse streamer would show best on the K-coronameter while a dense streamer would tend to show more prominently on the radioheliograph.

3.3. Brightness temperature

In order to determine the brightness temperature of the Sun, we need an absolute calibration of the heliograph. We have done this in two ways: (1) On one day (July 18) the heliograph was used to observe a strong source (Hercules A) whose flux density is well known, and thus the flux density scale was determined. (2) On the same day, using a radiometer on an aerial whose gain is known (McAlister and Labrum, 1967), we measured the integrated flux density of the Sun and found values of 2.4×10^{-22} and 6.2×10^{-22} W m^{-2} Hz^{-1} at 80 and 160 MHz respectively. Comparing these values with the results of integrating the radioheliograph maps shown in Figure 1, we determined the flux density scale.

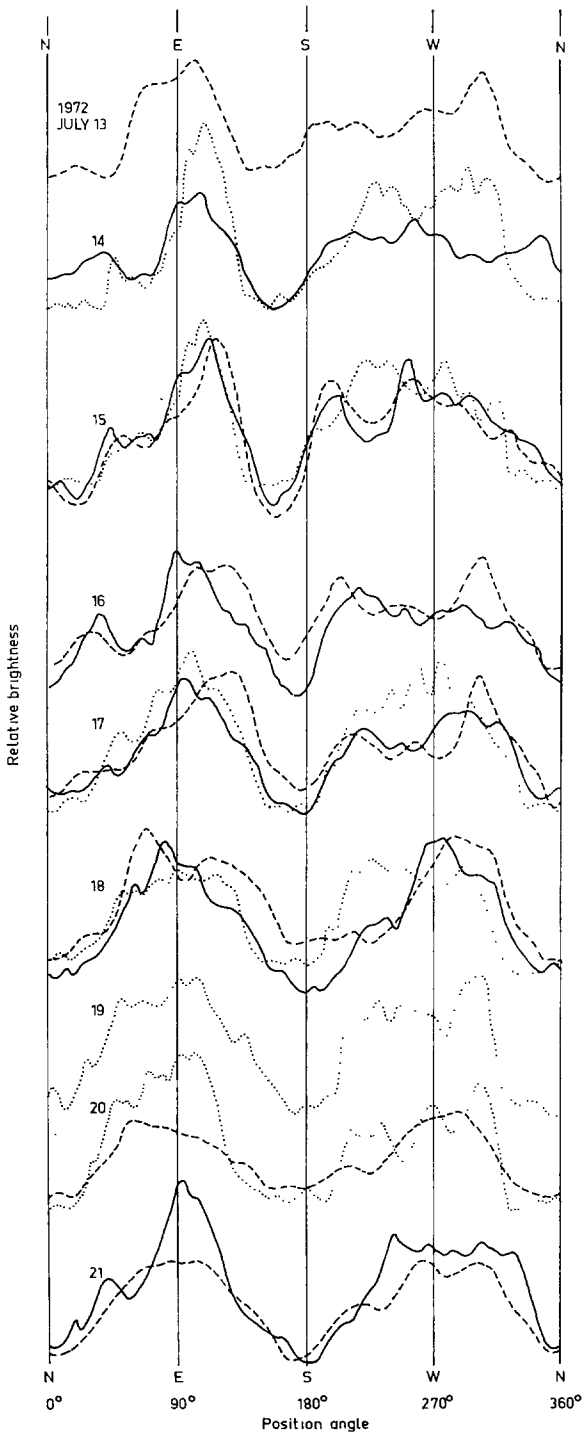

Fig. 2. Scans of coronal brightness as a function of position angle at fixed heights above the limb. *Full lines*: 160 MHz at 1.2 $R_\odot$; *dashed lines:* 80 MHz at 1.45 $R_\odot$; *dotted lines:* K-corona at 1.57 $R_\odot$. The radio observations (from Culgoora) were made near 02^h UT and the K-corona observations (from the High Altitude Observatory in Hawaii) were made at about 18^h UT on the previous day. The intensity scale is arbitrary for all data.

The two methods of calibration agreed to within 20%.* We have calibration data only for July 18, but as the Sun's total flux density remained constant over the interval from July 13 to 21 (*Quart. Bull. Solar Activity*, 1973) we were able to determine the scale factors for the other days. The day-to-day variation in scale factor was $\lesssim 25\%$.

Figure 1 includes the peak brightness temperature derived on each day. The temperatures at 80 MHz averaged about 10% larger than at 160 MHz, but this difference is less than the possible error in calibration of about 20%. The day-to-day changes in peak temperature at 160 MHz are quite small. At 80 MHz, the day-to-day changes were larger and were associated with the passage of the bright region across the disk from July 15 to 18.

4. Interpretation

4.1. Coronal holes at radio frequencies

We now consider the implications of the coronal holes being apparent on the 80 and 160 MHz contour maps. The radio brightness depends on refraction and scattering in the corona and on the number of electrons and the kinetic temperature along the ray path. To simplify this discussion, we will consider only the coronal holes near the centre of the disk (as on July 20–21) when refraction and scattering are minimal. We will also assume that the material in the coronal hole has a constant temperature which differs from that in the nearby 'normal' corona, and we will allow for the possibility that the ray may penetrate into the chromosphere before reaching the reflection level. Then the brightness temperature is

$$T_b = T_c(1 - e^{-\tau_c}) + T_{ch}e^{-\tau_c}, \tag{1}$$

where τ is the optical depth, the subscripts c and ch refer to the corona and chromosphere respectively, and we have assumed that $\tau_{ch} \gg 1$ (e.g. Smerd, 1950). If $\tau_c \gg \gg (T_{ch}/T_c) \approx 10^{-2}$, which is always true at 80 and 160 MHz, then the term involving T_{ch} is negligible. Thus

$$T_b \approx T_c(1 - e^{-\tau_c}). \tag{1'}$$

The differential optical depth $d\tau$ is

$$d\tau = CN_e^2 T^{-3/2} f^{-2}\, ds, \tag{2}$$

where ds is the differential pathlength and the proportionality factor C depends only weakly on f and T. Then for a given f and constant T_c we obtain from (2)

$$\tau_c \propto \int N_e^2\, ds \sim \langle N_e^2 \rangle L \sim \langle f_p^4 \rangle L, \tag{3}$$

where L is the effective pathlength in the region of the corona which contributes most to the optical depth.

* As reported at the 1973 General Assembly of the IAU, the widely used flux density scale of Conway *et al.* (1963) is probably about 20 % too low at low frequencies. If this is confirmed, the values of flux density and temperature derived in this paper should be increased by about 20 %.

For an electron density model, we take Newkirk's (1961) spherically symmetric corona multiplied by a factor D, i.e.

$$N_e = 4.2 \times 10^4 \, D e^{Q/R}, \tag{4}$$

where R is the radial distance in solar radii, $D \approx 0.1$ to 0.5 for a coronal hole (Munro and Withbroe, 1972; Perry and Altschuler, 1973), $D = 2$ for the average active region observed by Newkirk, and $D \approx 10$ for a dense streamer (Newkirk, 1967; Saito and Owaki, 1967). In addition,

$$Q = (GM_\odot \mu m_H)/(R_\odot k T_c) \quad \text{(units of } R_\odot), \tag{5}$$

where G is the gravitational constant, $M_\odot$ is the solar mass, μ is the mean molecular mass of the coronal material, m_H is the mass of the hydrogen atom, and k is Boltzmann's constant. In the electron density model of Equation (4), hydrostatic equilibrium applies and the scale height H is

$$H \equiv -N_e \Big/ \frac{dN_e}{dR} = \frac{R^2}{Q}. \tag{6}$$

In his model, Newkirk (1961) takes $Q = 10$ – i.e., the coronal temperature T_c is assumed to be constant at 1.4×10^6 K.

Figure 3 shows the variation of T_b with D, calculated from Equations (1′), (4), and a numerical integration of Equation (2). We can understand the main features of the curves as follows.

(1) If the ray path at a given radio frequency penetrates into the chromosphere, then the values of N_e and L appropriate for Equation (3) are the electron density and half the scale height *in the lowest corona* respectively. (Half, rather than the full scale height is used because N_e^2 falls by a factor of $1/e$ in half of a density scale height.) H and hence L are independent of D at the bottom of the corona, so from Equations (3) and (4) we have $\tau_c \sim \langle N_e^2 \rangle \sim D^2$. Therefore, τ_c decreases rapidly with decreasing D and as soon as $\tau_c \lesssim 1$, the brightness temperature drops rapidly. This occurs near $D = 0.5$ and 0.12 for 160 and 80 MHz respectively.

(2) If the ray at a given frequency reflects from the plasma level in the corona, then the value of f_p appropriate for Equation (3) is the radio frequency and L is the full (because of the double pass of the ray) scale height *at the plasma level.* In this case $\langle f_p^4 \rangle$ is independent of D; however, a decrease in D will cause the plasma height to be somewhat lower and hence (by Equation (6)) the scale height will be slightly smaller. Thus τ is only a weak function of D, so the optical depth and hence the brightness temperature decreases only slowly with decreasing D. In Figure 3, the slope of the 80 MHz curves for $T > 1.0 \times 10^6$ K is due to this effect.

Consideration of the curves of Figure 3 allows us to draw the following inferences.

(1) At 160 MHz the lowered brightness temperature in coronal holes cannot be due to a density decrease alone unless the hole is sufficiently underdense to allow the ray to penetrate into the chromosphere – i.e., inside the hole f_p must be less than 160 MHz at the chromospheric boundary. In the model used to calculate Figure 3 the chromo-

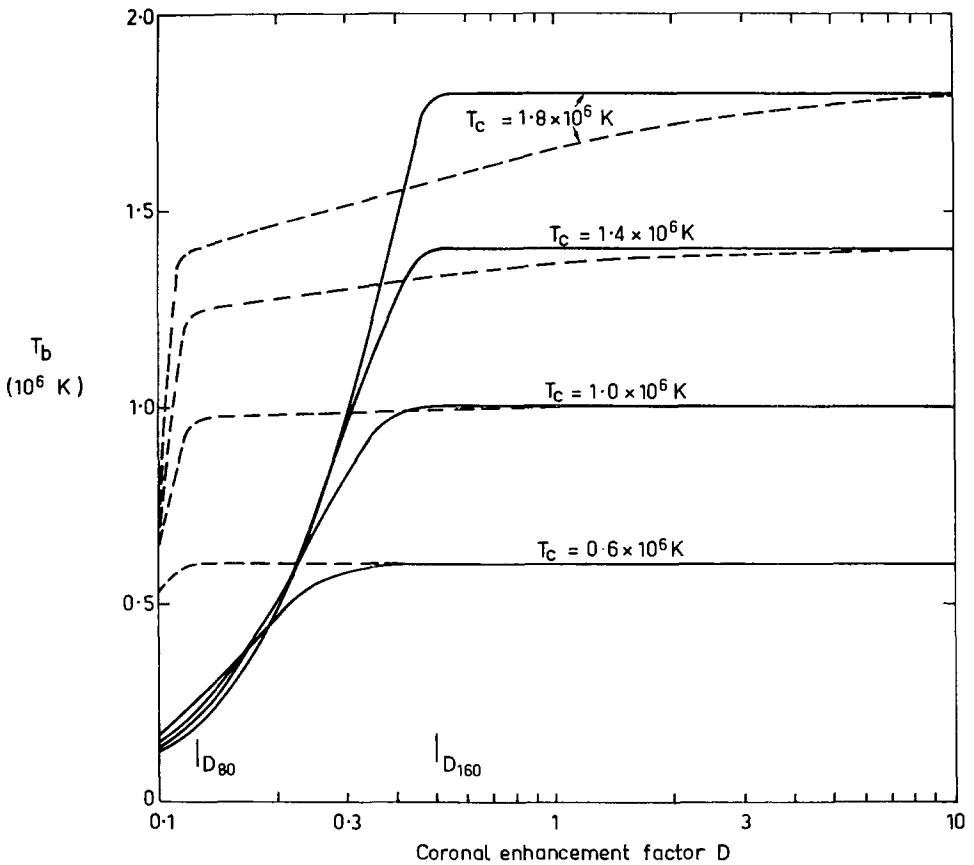

Fig. 3. Calculated brightness temperatures at the centre of the disk as a function of coronal enhancement at 80 MHz (dashed lines) and 160 MHz (full lines) for several kinetic temperatures. The coronal density is assumed to be Newkirk's (1961) spherically symmetric component multiplied by the factor D. When $D < D_{160}$ (D_{80}) the 160 (80) MHz plasma level is in the chromosphere.

spheric boundary is placed at a height of 20000 km and a 160 MHz ray will penetrate into the chromosphere if $D \lesssim 0.5$.

(2) 80 MHz rays will not enter the chromosphere unless $D \lesssim 0.1$, which seems unlikely. If $T_c \gtrsim 1.4 \times 10^6$ K, the 80 MHz brightness temperature in a hole can be lowered by 10–20% by a density decrease alone. However, as shown on Figure 1, the measured brightness temperature in the vicinity of coronal holes is only $\sim 1.0 \times 10^6$ K. Therefore we deduce that the radio manifestation of the observed coronal holes *is not* due to a density decrease alone.

(3) A decrease in temperature in a hole, even if not accompanied by a decrease in density, would lower the radio brightness. But it could not explain the corresponding observations in UV and white light (e.g. Altschuler *et al.*, 1972; Withbroe, 1972).

We conclude from these three inferences that the radio manifestations of coronal holes must be due to a decrease in both temperature and density.

We now estimate the temperature and relative density inside the hole near the disk centre on July 20–21 from the observed brightness temperatures. We find from Figure 1b that, at 80 MHz, the brightness temperature outside the hole was $T_{b,o} \approx 1.0 \times 10^6$ K and inside the hole $T_{b,i} \approx 0.8 \times 10^6$ K. At 160 MHz these values are about 1.0×10^6 and 0.6×10^6 K respectively. As discussed above, the observations may have a calibration error of $\sim 20\%$, but taking the observed brightness temperatures at face value and referring to Figure 3 we find that the 80 MHz brightness temperatures would be essentially the kinetic temperatures outside and inside the holes – i.e., $T_{c,o} \approx 1.0 \times 10^6$ K and $T_{c,i} \approx 0.8 \times 10^6$ K. At 160 MHz the brightness temperature in the hole, $T_{b,i} \approx$ $\approx 0.6 \times 10^6$ K, would imply that the coronal enhancement factor inside the hole, D_i, was about 0.2 to 0.3.

4.2. Coronal enhancements at radio frequencies

In contrast to the coronal holes, the enhancements seen on UV spectroheliograms (and microwave maps) are manifested only weakly, if at all, on the 80 and 160 MHz maps. Most coronal enhancements are known to be regions of high density and temperature that are confined to the low corona by the magnetic fields of new, hot active regions. However, 80 and 160 MHz rays do not penetrate to the low corona except in regions of depleted density. This is especially pronounced near the limb, where refraction keeps the rays well above the plasma level. But even near the centre of the disk, the 80 and 160 MHz bright regions are only weakly correlated with bright features on the UV maps. Axisa *et al.* (1971) found a similar lack of correspondence between plages and radio flux increases at 169 MHz. We take this to imply that the temperature in the middle corona above the new, hot active regions is approximately the same as average. Withbroe (1972) found that the temperature gradient immediately above active regions is considerably steeper than average, causing the middle coronal temperature to be only slightly higher than average. Our results support his conclusions.

4.3. Coronal helmets at radio frequencies

There are some bright features on the 80 MHz maps (especially the feature crossing the disk from July 15 to 18 (Figure 1a)) that are present, although weaker, at 160 MHz. These probably correspond to the 'radio flux increases' observed by Axisa *et al.* (1971) on one-dimensional scans at 169 MHz. Axisa *et al.* found that the longitude of radio flux increases corresponded (in at least 60% of the cases) to the longitude of a quiescent filament. Our data confirm this relationship; indeed, the brightest feature on the maps of July 13 to 18 seems to lie directly above a very long ($\sim 0.6\ R_\odot$) quiescent filament which is remote from active regions. For less prominent radio bright regions, the relationship is not so clear; some may be associated with quiescent filaments, some with active region streamers and in one or two cases, with a weak, non-thermal source (e.g. July 21).

It is well known that quiescent filaments usually lie at the base of coronal helmets (e.g. Billings, 1966). We can use the observed radio brightness to estimate the tempera-

ture and density in the helmets as we did for the coronal holes. On July 15, when it was near the centre of the disk, the brightness temperature in the helmet (almost directly above the filament) was $T_b \simeq 1.4 \times 10^6$ K at 80 MHz. As seen from Figure 3, this must be nearly the same as the kinetic temperature, at least in an enhanced density region such as a helmet. At 160 MHz there were two sources with approximately equal brightness temperatures ($T_b \approx 1.1 \times 10^6$ K) which straddled the filament (see Figure 1a).

These observations lend support to the model of a coronal helmet given by Pneuman (1972). In Pneuman's model, at a height near the top of the helmet (where the 80 MHz plasma level presumably occurs), the temperature and density maximize at a location directly over the filament. At a lower height (where the 160 MHz plasma level presumably occurs) there is a cold filament surrounded by an underdense filament cavity, much of which is cooler than the enveloping coronal helmet. Thus the filament and cavity, with a lower brightness temperature than the surroundings, can split the region, resulting in a double source, as was observed at 160 MHz. Pneuman's Figures 6 and 7 give values which fit our observations reasonably well, except that the observed brightness temperature in the two peaks at 160 MHz ($\sim 1.1 \times 10^6$ K) is lower than the value of 1.4×10^6 K predicted from the 80 MHz brightness. Two possible causes for this discrepancy are (1) the 20% uncertainty in our absolute flux calibration, and (2) the helmet temperature may increase with height faster than given by Pneuman's model.

It is interesting to note that none of the type I or type III bursts which occurred between July 13 and 18 were located near the position of the helmet.

5. Conclusions

We summarize the major results of this paper as follows.

(1) There is a close association between dark regions seen on metre-wavelength radio maps and the coronal holes identified by UV, X-ray and white-light observations. Radio observations can be used to deduce the density and temperatures in the holes.

(2) Active regions are not manifested on the radio maps, implying that the temperature in the middle corona above the active regions is nearly the same as elsewhere and that the temperature gradient near the top of the coronal enhancement is steeper than average.

(3) Coronal helmets above quiescent filaments cause the bright regions on the radio maps. The model of coronal helmets by Pneuman (1972) provides an explanation for most of the observed features.

Acknowledgements

We thank R. T. Hansen and S. F. Hansen for extensive cooperation and for supplying the K-coronameter scans in advance of publication, and D. J. McLean and S. F. Smerd for enlightening discussions and criticism.

References

Altschuler, M. D., Trotter, D. E., and Orrall, F. Q.: 1972, *Solar Phys.* **26**, 354.
Aubier, M., Leblanc, Y., and Boischot, A.: 1971, *Astron. Astrophys.* **12**, 435.
Avignon, Y. and Le Squeren-Malinge, A. M.: 1961, *Compt. Rend.* **253**, 2859.
Axisa, F., Avignon, Y., Martres, M. J., Pick, M., and Simon, P.: 1971, *Solar Phys.* **19**, 110.
Billings, D. E.: 1966, *A Guide to the Solar Corona*, Academic Press, N.Y., p. 65.
Conway, R. G., Kellermann, K. I., and Long, R. J.: 1963, *Monthly Notices Roy. Astron. Soc.* **125**, 261.
Hansen, R. T., Garcia, C. J., Hansen, S. F., and Loomis, H. G.: 1969, *Solar Phys.* **7**, 417.
Hansen, S. F., Hansen, R. T., and Garcia, C. J.: 1972, *Solar Phys.* **26**, 202.
Hobbs, R. W., Jordan, S. D., and Webster, W. J. Jr.: 1973, *Nature Phys. Sci.* **243**, 48.
Kundu, M. R.: 1971, *Solar Phys.* **21**, 130.
Leblanc, Y.: 1970, *Astron. Astrophys.* **4**, 315.
McAlister, K. R. and Labrum, N. R.: 1967, *Proc. Inst. Radio Elec. Engrs. Australia* **28**, 291.
Munro, R. H. and Withbroe, G. L.: 1972, *Astrophys. J.* **176**, 511.
Newkirk, G. Jr.: 1961, *Astrophys. J.* **133**, 983.
Newkirk, G. Jr.: 1967, *Ann. Rev. Astron. Astrophys.* **5**, 213.
Perry, R. M. and Altschuler, M. D.: 1973, *Solar Phys.* **28**, 435.
Pneuman, G. W.: 1972, *Astrophys. J.* **177**, 793.
Quarterly Bulletin Solar Activity: 1973, IAU, No. 179.
Saito, K. and Owaki, N.: 1967, *Publ. Astron. Soc. Japan* **19**, 535.
Sheridan, K. V.: 1970, *Proc. Astron. Soc. Austr.* **1**, 304.
Sheridan, K. V., Labrum, N. R., and Payten, W. J.: 1973, *Proc. IEEE* **61**, 1312.
Smerd, S. F.: 1950, *Austr. J. Sci. Res. Series A* **3**, 34.
Solar-Geophysical Data: 1972, IER-FB 337, Part 1, U.S. Dept. of Commerce, Boulder, Colo.
Vaiana, G. S., Davis, J. M., Giacconi, R., Krieger, A. S., Silk, J. K., Timothy, A. F., and Zombeck, M.: 1973a, *Astrophys. J. Letters* **185**, L47.
Vaiana, G. S., Krieger, A. S., and Timothy, A. F.: 1973b, *Solar Phys.* **32**, 81).
Withbroe, G. L.: 1972, *Solar Phys.* **25**, 116.
Withbroe, G. L., Dupree, A. K., Goldberg, L., Huber, M. C. E., Noyes, R. W., Parkinson, W. H., and Reeves, E. M.: 1971, *Solar Phys.* **21**, 272.